Available online at www.sciencedirect.com
SCIENCE DIRECT®
International Journal of Heat and Mass Transfer 48 (2005) 83–103
International Journal of HEAT and MASS TRANSFER
www.elsevier.com/locate/ijhmt

Condensation induced non-condensables accumulation in a non-vented vertical pipe

Vladimir D. Stevanovic [a,*], Zoran V. Stosic [b], Uwe Stoll [b]

[a] University of Belgrade, Kraljice Marije 16, 11000 Belgrade, Serbia and Montenegro
[b] Framatome ANP GmbH, P.O. Box 3220, D-91050 Erlangen, Germany

Received 24 May 2004

Abstract

At the end of the year 2001 the radiolytic gases hydrogen and oxygen accumulated and exploded in non-vented steam pipelines at two nuclear power plants. The HELIO code has been developed for the numerical simulation and analyses of these incidents and as a support to the prescription of safety measures. This paper presents modelling and numerical approach, verification and results of the two-dimensional module of the HELIO code for the conditions of hydrogen–oxygen accumulation in a vertical pipe closed at the top. The results show a dynamics of hydrogen–oxygen accumulation, formation and propagation of the concentration front, gas mixture natural convection due to concentration and temperature imposed buoyancy forces and gas mixture–liquid film interface shear. The verification against plant data and for the common problem of steam condensation in the presence of air is presented.

Keywords: Condensation; Hydrogen; Noncondensable; Accumulation; Numerical simulation

1. Introduction

A hydrogen and oxygen accumulation and a mixture explosion occurred in non-vented steam pipelines of safety systems in the nuclear power plants Hamaoka in Japan [1] and Brunsbuettel in Germany [2,3] at the end of 2001. Although the presence of these radiolytic and non-condensable gases in the main steam of Boiling Water Reactors has been well known, their accumulation to explosive mixtures has not been expected. These incidents revealed a new problem that must be fully understood and investigated in order to provide plant safety. The hydrogen and oxygen are present in coolants of light water nuclear reactors during normal operation. They are produced by the radiolytic decomposition of water exposed to the nuclear fuel radiation [4].

Measurements have shown that in the main steam of the Boiling Water Reactor the mass fraction of hydrogen and oxygen is approximately 22.5×10^{-6}. The molar ratio of hydrogen to oxygen is 2:1, which means 2.5×10^{-6} of hydrogen mass fraction and 20×10^{-6} of oxygen. The hydrogen and oxygen concentrations could be further substantially increased if steam condenses in non-vented pipes or components. Steam is condensed and drained, while the concentration of remaining non-condensables increases. After the time periods of several days, weeks or months even an explosive mixture of hydrogen and oxygen could be reached.

* Corresponding author. Tel.: +381 11 3370 561; fax: +381 11 3370 364.
E-mail address: estevavl@eunet.yu (V.D. Stevanovic).

0017-9310/$ - see front matter © 2004 Elsevier Ltd. All rights reserved.
doi:10.1016/j.ijheatmasstransfer.2004.08.006

Nomenclature

A	area, m^2
c_p	specific heat, $J\,kg^{-1}\,K^{-1}$
D	diffusion coefficient, $m^2\,s^{-1}$, pipe diameter, m
D_h	hydraulic diameter, m
f	friction coefficient
g	mass fraction, gravity, $m\,s^{-2}$
H	Henry's constant
h	heat transfer coefficient, $W\,m^{-2}\,K^{-1}$, specific enthalpy, $J\,kg^{-1}$
j_{con}	condensation mass flux, $kg\,m^{-2}\,s^{-1}$
j_a	absorption mass flux, $kg\,m^{-2}\,s^{-1}$
k	thermal conductivity, $W\,m^{-1}\,K^{-1}$
k_L	mass transfer coefficient, $m\,s^{-1}$
L	length, m
M	molar mass, $kg\,kmol^{-1}$
p	pressure, Pa
p_c	partial pressure of gas mixture component, Pa
R	pipe radius, m
Re	Reynolds number
r	radial co-ordinate, m
T	temperature, K, °C
t	time, s
u, v	velocity components, $m\,s^{-1}$
V	volume, m^3
V_i	molecular volume, Eq. (42)
x	molar fraction, co-ordinate, m
y	co-ordinate, m

Greek symbols

α	volume fraction
Γ_{con}	rate of condensation, $kg\,m^{-3}\,s^{-1}$
Γ_a	rate of absorption, $kg\,m^{-3}\,s^{-1}$
δ	liquid film thickness, m
λ	latent heat of condensation, $J\,kg^{-1}$
μ	dynamic viscosity, $kg\,m^{-1}\,s^{-1}$
ν	kinematic viscosity, $m^2\,s^{-1}$
ρ	density, $kg\,m^{-3}$
τ	shear stress, $N\,m^{-2}$

Subscripts

atm	parameter of the surrounding atmosphere
c	non-condensable component of the gas mixture
CV	control volume
H_2	hydrogen
i	liquid film surface, gas mixture–liquid film interface
in	insulator
O_2	oxygen
w	wall
1	liquid film surface
2	gas mixture

Superscript

n	trigger for Cartesian ($n = 0$) or cylindrical ($n = 1$) co-ordinates in governing equations

Since the problem was recognised recently, results about condensation induced radiolytic gases accumulations in the open literature are limited. The plant evidences of the hydrogen and oxygen accumulation, based on the industrial type measurements applied in power plants, are reported in [2,3]. Small diameter vertical pipes open at the bottom and closed at the top are especially prone to radiolytic gases accumulation, as well as other higher elevated parts of non-vented pipelines. The Hamaoka plant incident initiated an experimental investigation of the non-condensables accumulation in a complex steam pipeline [1]. The pipeline consisted of several horizontal and vertical segments and elbows. For safety reasons, the helium was used instead of hydrogen. In order to speed up the process hundred and thousand times higher initial concentration of helium and oxygen were applied than those caused by the radiolytic decomposition of steam in the nuclear power plant. Also, the accumulation process was simulated with the application of the commercial CFD (Computational Fluid Dynamic) code and with the built-in simplified model of the process.

The hydrogen and oxygen accumulation within non-vented pipes and volumes is driven by coupled thermal–hydraulic and diffusion phenomena, such as steam condensation in the presence of non-condensables, condensate drainage, non-condensables absorption and degassing at the liquid film surface, gas mixture natural convection due to concentration and temperature induced buoyancy forces and due to gas mixture shear at the moving liquid film surface [5,6]. Some aspects of this new complex problem have been the main goals of some previous investigations, such as vapour condensation in the presence of non-condensables, and hydrogen accumulation in large volumes. Condensation of vapour in the presence of non-condensable gases is an important process for the efficiency of various condensers in power and chemical industry. The heat transfer coefficient is significantly reduced in the presence of non-condensables due to the non-condensables concentration increase at the condensing surface [7–14]. Power plant condensers, heat exchangers, condensers within the passive safety systems of advanced nuclear power plants are some examples of the equipment which operational effi-

ciency depends on this process [15,16]. The second group of investigations has been directed towards the prediction of non-condensable hydrogen transport and accumulation in large volumes in the mixture with steam or steam and air [17,18]. Namely, during a hypothetical severe accident in the nuclear power plant, a substantial amount of hydrogen can be generated from a chemical reaction between the zirconium cladding of the nuclear fuel elements and the high temperature water steam, as well as from the core–concrete interactions after a lower head failure of the nuclear reactor vessel. Such generated hydrogen may be transported into the compartments in the containment building, and has the potential to threaten the containment integrity by over-pressurizing from global burning or explosions.

In order to investigate all aspects of the complex process of hydrogen and oxygen accumulation in non-vented steam pipelines, the multi-dimensional thermal–hydraulic and physico-chemical in-house code HELIO has been developed [5,6]. In this paper, modelling and numerical approach, verification and results of the two-dimensional module of the HELIO code are presented. Section 3 of the paper presents modelling approach. The HELIO code model governing equations are based on the mass, momentum and energy conservation of the mixture of steam, hydrogen and oxygen, as well as on the conservation equations for hydrogen and oxygen mass fractions (a separate conservation equation for each gas mixture component). The condensate liquid film flow is treated according to the Nusselt theory. Laminar flow condition is considered due to the low liquid film and gas mixture Reynolds numbers. Gas mixture partial pressures are calculated according to the Dalton's law, while the Henry's law is applied for the prediction of non-condensables absorption at the liquid film surface. The heat flux from the gas mixture to the environment is calculated by solving the two-dimensional transient heat conduction in the pipe's wall and insulator, where the coefficient of heat transfer from the outer insulator surface to the surrounding atmosphere is prescribed. Section 4 outlines a numerical solution procedure for the developed model, based on the SIMPLE type numerical method [19] modified for the conditions of two-phase flow [20]. Section 5 presents numerical results of the hydrogen and oxygen accumulation in a vertical non-vented pipe open at the bottom and closed at the top (the configuration that is common at the plant). Obtained transient results show gas mixture temperature fields, hydrogen and oxygen mass fraction fields, propagation of the accumulated non-condensables front from the top to the bottom of the pipe, as well as gas mixture convection induced by the steam condensation, by buoyancy forces due to the non-uniform concentration and temperature fields and by interfacial shear at the liquid film surface. A separate case of the hydrogen and oxygen accumulation in a long vertical pipe with a large diameter is simulated. The temperature transient at the pipe's top for the real-time period of one month is calculated and compared with the plant-measured data. Also, in order to demonstrate the HELIO code versatility, usability and appropriateness of the applied models to predict the condensation in the presence of non-condensables, which is one of the crucial phenomena in the process of non-condensables accumulation, a steam-air flow over a uniformly cooled vertical plate is simulated.

The numerical investigation in this paper is unique since it comprises all important phenomena and effects that are involved in the process of condensation induced non-condensables accumulation. In the previous CFD investigation of the Hamaoka incident [1], the applied three-dimensional model was simplified in a sense that the presence of the draining condensate film was ignored, the energy equation was omitted (instead, it was assumed that the temperature of the steam, helium and oxygen mixture is determined with the saturation temperature of steam at its partial pressure), and both helium and oxygen were observed as a single non-condensable gas. The models developed mainly for the prediction of the condensation heat transfer coefficient in the presence of non-condensables are limited only to one-dimensional (examples of which are papers [10,11,13]), or plane and boundary layer steady-state flows [12,14,15]. The transient models used for the prediction of hydrogen accumulation in large volumes [17,18] have the potential of non-condensables accumulation prediction, but their use in the pipelines geometries and an upgrading regarding the condensate film presence and liquid film–gas mixture interactions is not straightforward.

The incidents of hydrogen accumulation and explosions at two nuclear power plants [1,2] under normal operating conditions imposed a new problems and questions to the nuclear regulative commissions, licensing procedures and safety measures. There are activities to pose a condensation induced hydrogen accumulation as a standard benchmark problem. The well-founded and verified methodology and results are a contribution to these activities. The numerical simulations can support the optimisation of the temperature measurement locations that are used at the plant to indicate the radiolytic gases accumulation. Also, numerical simulations can replace expensive experimental investigations.

2. Problem statement

Fig. 1 presents a vertical pipe closed at the top and open at the bottom. Although the pipe is isolated, the heat loss to the surrounding cannot be totally eliminated, and some amount of steam condenses on the wall. The liquid film of condensate is drained due to gravity.

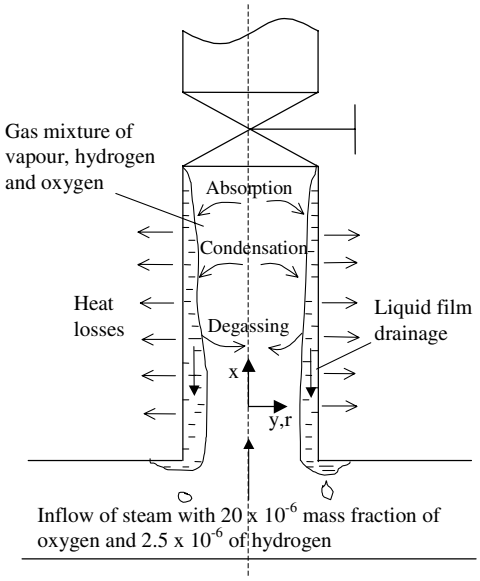

Fig. 1. Steam condenses in the presence of non-condensable hydrogen and oxygen in a vertical pipe. Liquid film is formed on the wall and drains due to gravity. The hydrogen and oxygen accumulate within the pipe.

The condensed steam is replaced by the inflow of mixture of steam and small amount of radiolytic gases at the junction of the vertical pipe with the surrounding system. The intensity of steam condensation on the isolated pipe's wall is small, but, nevertheless, after some time, the non-condensables concentration in the vertical pipe will increase considerably, and even an explosive hydrogen–oxygen concentration could be reached. Some amount of non-condensables is absorbed on the liquid film surface and removed with the drained condensate, but, the rate of this effect is smaller than the inflow of non-condensables at the pipe bottom.

The modelling of thermal–hydraulic and physico-chemical processes presented in Fig. 1 has to take into account several phenomena and effects:

(a) The transport of hydrogen and oxygen and its accumulation (the numerical results will show that the accumulation starts at the pipe top and propagates downwards) are the result of combined effects of non-condensables diffusion and mixture convection. The gas mixture convection is determined with the steam condensation and its replenishment from the pipe open bottom, with the interfacial drag between the gas mixture and the draining liquid film, and with the buoyancy forces caused by non-uniform fields of gas mixture temperature and non-condensables concentration.

(b) It is assumed that the film condensation takes place at the inner pipe's wall. The condensation occurs when the temperature of the inner wall surface is lower than the steam saturation temperature determined with the steam partial pressure. Due to the low heat flux rates from the insulated pipe to the surrounding atmosphere, the condensation rate is low, and consequently, the liquid film thickness is low (in the section with numerical results presentation it will be shown that the liquid film thickness is of the order of tens of microns). The dropwise condensation is not considered. But, due to the thin liquid film draining, it could not be completely excluded that the liquid film may become unstable to cover the whole pipe innerwall surface and dropwise condensation may occur. The heat transfer coefficient under dropwise condensation is higher than in case of film condensation, but for here analyzed conditions this effect is not important since the resistance of the pipe insulator is predominant and determines the overall heat transfer coefficient. Hence, the calculated amount of condensed steam would not practically differ between cases of film and dropwise condensation. In case of dropwise condensation, a thermal–hydraulic interaction of the draining drops and the gas mixture convection is complicated by the intermittent time-dependent character of the dropwise condensation and the uncertainty associated with the location of nucleation sites and the time when the largest droplet will start its movement downstream. The approximation of dropwise condensation with the film condensation (under the same heat loss rates) should be regarded as the averaged representation of the intermittent droplets drainage. Further, it could be stipulated that for the long time periods (several days or even months) and longer pipe lengths (several meters and longer) the time-averaged drainage of drops in the dropwise condensation should impose nearly the same influence to the gas mixture flow as the liquid film drainage.

(c) Absorption or degassing of non-condensables at the liquid film surface takes place. It should be noted that besides the non-condensables absorption, it is also possible to have removal of non-condensable gases from the liquid film to the steam-non-condensables mixture. As it will be explained in the next sections, a direction of the non-condensables transport at the liquid film surface is determined with the dependence of the non-condensables saturation concentration in the thin liquid film on the film temperature and on the non-condensables concentration in the gas mixture (according to the Henry's law [21]).

3. Modelling approach

Governing equations are written for the mixture of steam, hydrogen and oxygen, by assuming that these chemical species are in thermal (same temperature) and mechanical (same velocity) equilibrium. Since the pipe geometry and boundary conditions are axisymmetric, as presented in Fig. 1, the governing equations are written in two-dimensional cylindrical coordinates. The

same set of equations can be easily converted to a form that models two-dimensional plane flow with the introduction of the appropriate parameter n as shown below.

3.1. Mass, momentum and energy conservation equations for the gas mixture

Mass conservation

$$\frac{\partial(\alpha_2\rho_2)}{\partial t}+\frac{1}{y^n}\frac{\partial(\alpha_2\rho_2 y^n v_2)}{\partial y}+\frac{\partial(\alpha_2\rho_2 u_2)}{\partial x}=-\sum_{m=1}^{M}\Gamma_m \tag{1}$$

Momentum conservation

y,r-direction

$$\begin{aligned}&\frac{\partial(\alpha_2\rho_2 v_2)}{\partial t}+\frac{1}{y^n}\frac{\partial(\alpha_2\rho_2 y^n v_2^2)}{\partial y}+\frac{\partial(\alpha_2\rho_2 u_2 v_2)}{\partial x}\\&\quad=-\alpha_2\frac{\partial p}{\partial y}+\frac{2}{y^n}\frac{\partial}{\partial y}\left(\alpha_2\mu_2 y^n\frac{\partial v_2}{\partial y}\right)+\frac{\partial}{\partial x}\left(\alpha_2\mu_2\frac{\partial u_2}{\partial y}\right)\\&\qquad+\frac{\partial}{\partial x}\left(\alpha_2\mu_2\frac{\partial v_2}{\partial x}\right)-\frac{2\alpha_2\mu_2 n v_2}{y^2}-\sum_{m=1}^{M}\Gamma_m v_i-\alpha_2\rho_2 g_y\end{aligned} \tag{2}$$

x-direction

$$\begin{aligned}&\frac{\partial(\alpha_2\rho_2 u_2)}{\partial t}+\frac{1}{y^n}\frac{\partial(\alpha_2\rho_2 y^n u_2 v_2)}{\partial y}+\frac{\partial(\alpha_2\rho_2 u_2^2)}{\partial x}\\&\quad=-\alpha_2\frac{\partial p}{\partial x}+\frac{1}{y^n}\frac{\partial}{\partial y}\left(\alpha_2\mu_2 y^n\frac{\partial v_2}{\partial x}\right)\\&\qquad+\frac{1}{y^n}\frac{\partial}{\partial y}\left(\alpha_2\mu_2 y^n\frac{\partial u_2}{\partial y}\right)+2\frac{\partial}{\partial x}\left(\alpha_2\mu_2\frac{\partial u_2}{\partial x}\right)\\&\qquad-\sum_{m=1}^{M}\Gamma_m u_i-\alpha_2\rho_2 g_x\end{aligned} \tag{3}$$

Mixture energy conservation

$$\begin{aligned}&\frac{\partial(\alpha_2\rho_2 c_{p,2}T_2)}{\partial t}+\frac{1}{y^n}\frac{\partial(\alpha_2\rho_2 c_{p,2}y^n v_2 T_2)}{\partial y}+\frac{\partial(\alpha_2\rho_2 c_{p,2}u_2 T_2)}{\partial x}\\&\quad=\frac{1}{y^n}\frac{\partial}{\partial y}\left(\alpha_2 y^n k_2\frac{\partial T_2}{\partial y}\right)+\frac{\partial}{\partial x}\left(\alpha_2 k_2\frac{\partial T_2}{\partial x}\right)-\sum_{m=1}^{M}\Gamma_m h_m\end{aligned} \tag{4}$$

In Eqs. (1)–(4) parameter $n = 1$ holds for axisymmetric flow (cylindrical co-ordinates $x - r$) and $n = 0$ for plane flow (Cartesian co-ordinates $x - y$). In case of axisymmetric flow the y axis is identical to the radius r measured from the axis of symmetry, as it is indicated in Fig. 1. Both cylindrical and Cartesian co-ordinates are used in the numerical simulation in this paper. The index 2 denotes the gas mixture of steam, hydrogen and oxygen. The parameters used in the above equations are gas mixture volume fraction α_2, gas mixture density ρ_2, gas mixture velocity components u_2 and v_2 in x and y (or r) direction respectively, temperature T_2, pressure p, interfacial mass transfer rate at the liquid film surface due to phase transition (condensation or evaporation in general case) or absorption/degassing Γ, dynamic viscosity μ_2, specific heat c_{p2}, thermal conductivity k_2, and enthalpy of species in interfacial transfer at the liquid film surface h_m (enthalpy of condensing saturated steam determined with the steam partial pressure, as well as corresponding enthalpies of absorbing or degassing hydrogen and oxygen).

The governing equations (1)–(4) are derived from [22] for the conditions of flow with variable density, viscosity and thermal conductivity. The gas mixture volume fraction α_2 is introduced in order to take into account the presence of two-phases—liquid film and gas mixture in the zone adjacent to the wall. In the discretized governing equations (the control volume discretization is applied, as described in section Numerical solution procedure) the gas mixture volume fraction equals 1 in all control volumes except in the volumes that comprise liquid film. Since very thin liquid films develop under stated low heat fluxes to the surrounding atmosphere, the liquid film is placed only in one column of control volumes adjacent to the pipe wall. Hence, the gas volume fraction is less than 1 only in these boundary control volumes on the pipe wall (under the condition that condensate film exists).

The volume fraction balance of the gas and liquid phase is

$$\alpha_1+\alpha_2=1 \tag{5}$$

where α_1 represents liquid film volume fraction.

The sum of interfacial mass transfer rates in Eq. (1) is written as

$$\sum_{m=1}^{M}\Gamma_m=\Gamma_{\mathrm{con}}+\Gamma_{a,\mathrm{H_2}}+\Gamma_{a,\mathrm{O_2}} \tag{6}$$

The steam condensation rate is denoted as Γ_{con}, while terms $\Gamma_{\mathrm{a,H_2}}$ and $\Gamma_{\mathrm{a,O_2}}$ represent absorption ($\Gamma_{\mathrm{a,c}} > 0$, $c = \mathrm{H_2,O_2}$) or degassing ($\Gamma_{\mathrm{a,c}} < 0$) rates of hydrogen and oxygen per unit volume respectively. Components of the gas mixture and liquid phase interfacial velocities, where condensation, absorption or degassing takes place, are denoted with u_{i} and v_{i}.

3.2. Conservation equations for non-condensables mass fraction

Hydrogen and oxygen convection and diffusion in the gas mixture are treated for each component separately; therefore, the mass fraction conservation equation is written and solved for each non-condensable component.

$$\frac{\partial(\alpha_2\rho_2 g_{c,2})}{\partial t}+\frac{1}{y^n}\frac{\partial(\alpha_2\rho_2 y^n v_2 g_{c,2})}{\partial y}+\frac{\partial(\alpha_2\rho_2 u_2 g_{c,2})}{\partial x}=\frac{1}{y^n}\frac{\partial}{\partial y}\left[\alpha_2 y^n D_c\frac{\partial g_{c,2}}{\partial y}\right]+\frac{\partial}{\partial x}\left[\alpha_2\rho_2\rho_2 D_c\frac{\partial g_{c,2}}{\partial x}\right]-\Gamma_{a,c} \tag{7}$$

The index c in Eq. (7) denotes the non-condensable component (hydrogen or oxygen).The non-condensable mass fraction is denoted as g, while the diffusion coefficient of non-condensable component c in the mixture of gases is denoted with D_c.

3.3. Liquid film flow

The two-phase system presented in Fig. 1 is characterized with the thin condensate film drainage on the wall and the convection of steam – non-condensable mixture within the pipe. The liquid film flow is modelled with the well-known theoretical (and experimentally firmly approved) results.

The condensate drainage at the vertical wall is modelled according to the Nusselt solution of the condensation on the laminar liquid film. This approach is found to be appropriate since the liquid film thickness considered in this paper is of the order of several tens of microns, hence the inertia force in the liquid film can be neglected in comparison to the gravity and viscous force. If the liquid film is introduced at the top of the vertical plate and drained downward in the atmosphere of non-condensable stagnant gas, the velocity profile predicted with the Nusselt approach is reached after the entrance length longer than $100\cdot\delta_0$, where δ_0 represents steady-film thickness reached after the entrance length [24]. This means that for the liquid film thickness of several tens of microns, the entrance length along which the Nusselt velocity profile is reached is of the order of several centimetres—the length that is negligible compared to the pipe lengths of interest of several meters. The Nusselt approach is also derived under the assumption that there is no interfacial drag between the vapour phase and the liquid film. The theoretical results obtained with the perturbation method in [25] shows that the influence of the condensing steam (that is stagnant far from the condensing surface) on the liquid film velocity profile can be neglected if the heat capacity parameter $\varsigma = c_{p,1},(T_i - T_w)/\lambda$ is lower than 0.2, and the acceleration effect parameter $\xi = k_1(T_i - T_w)/(\mu_1\lambda)$ is close to zero (more exactly, it is approximated to by less than 0.1). Both conditions are satisfied in case of pure steam condensation. For instance, at the pressure of 7 MPa, and for the temperature difference across the condensate film of 0.5 K, the parameters have the following values $\varsigma = 5408\cdot 0.5/(1506\cdot 10^3)\approx 2\cdot 10^{-3}$ and $\xi = 0.565\cdot 0.5/(94\cdot 10^{-6}1506\cdot 10^3)\approx 2\cdot 10^{-3}$. The same conclusion can be derived for the condensation of steam from the mixture with non-condensable gases, since the thermo-physical parameters of the hydrogen–oxygen–steam mixture are of the same order of magnitude as parameters of the pure steam. But, here derived conclusion is not completely convincing, since the numerical results presented in this paper shows that non-uniform non-condensables concentration and gas mixture temperature fields induce buoyancy forces that exert gas mixture convection. Therefore, the steam does not condense from the stagnant volume of gas phase, instead the natural convection of the gas mixture exists. In order to estimate the influence of the steam natural convection on the liquid film flow, the interfacial shear stress is compared with the wall shear stress.

According to the Nusselt theory the wall shear stress is calculated as

$$\tau_w = \rho_1 g\delta_1 \tag{8}$$

In one-dimensional approach to the internal flow, the interfacial shear stress is calculated as [26]

$$\tau_i = f_i\frac{\rho_2(u_2-u_1)^2}{2} \tag{9}$$

The interfacial friction coefficient for laminar flow conditions is calculated as

$$f_i = \frac{16}{Re_2} \tag{10}$$

where the Reynolds number is calculated as

$$Re_2 = \frac{\rho_2 \mid u_2-u_1 \mid D_h}{\mu_2} \tag{11}$$

and the hydraulic diameter is $D_h \approx D$.

From Eqs. (8)–(11) the ratio of wall and interfacial shear stresses is derived as

$$\frac{\tau_w}{\tau_i} = \frac{\rho_1 g\delta_1 D}{8\mu_2(u_2-u_1)} \tag{12}$$

For the condensation of pure steam at the pressure level of 7 MPa in the pipe with diameter $D = 0.01$ m, the ratio in Eq. (12) is estimated as

$$\frac{\tau_w}{\tau_i} = \frac{740\cdot 9.81\cdot 50\cdot 10^{-6}\cdot 0.01}{8\cdot 20\cdot 10^{-6}\mid u_2-u_1\mid}\approx\frac{23}{\mid u_2-u_1\mid} \tag{13}$$

Numerical results presented in this paper shows that the difference of the gas mixture velocity (calculated by the numerical solution of the gas mixture two-dimensional flow) and the liquid film velocity (calculated according to the Nusselt theory) is surely lower than 0.5 m/s. Hence, according to the relation given with Eq. (13) the wall shear stress is at least 40 times higher than the interfacial shear stress. This conclusion supports the application of the Nusselt theory for the calculation of the liquid film thickness and velocity, for the conditions of pipe condensation investigated in this paper.

According to the Nusselt theory the liquid film thickness is determined as [22–24]

$$\delta_1 = \left(\frac{3\nu_1^2 Re_1}{g}\right)^{1/3} \tag{14}$$

where

$$Re_1 = \frac{u_1\delta_1}{\nu_1} \tag{15}$$

and

$$u_1\delta_1 = \frac{1}{\rho_1}\int_L j_{con}\,dx \tag{16}$$

Liquid film thickness δ_1, calculated with Eq. (14), is the local value at the downward distance L from the liquid film incipient. The integral on the r.h.s. of Eq. (16) calculates the sum of steam that is condensed on the liquid film from its beginning up to the downward length L per unit width of the liquid film perimeter, Fig. 2. The calculation of the liquid film parameters is performed in the following order. First, the r.h.s. of Eq. (16) is calculated. Than, the value of $(u_1\delta_1)$ is introduced in Eq. (15) and the liquid film Reynolds number is calculated. Finally, the liquid film thickness is calculated with Eq. (14).

The liquid film surface velocity is the liquid film maximum velocity and it is determined with [22–24]

$$u_{1,i} = \frac{3}{2}u_1 \tag{17}$$

and it is coupled with the gas mixture velocity under no slip conditions at the film surface

$$u_2(r = R) = u_{1,i} \quad \text{and} \quad v_2(r = R) = 0 \tag{18}$$

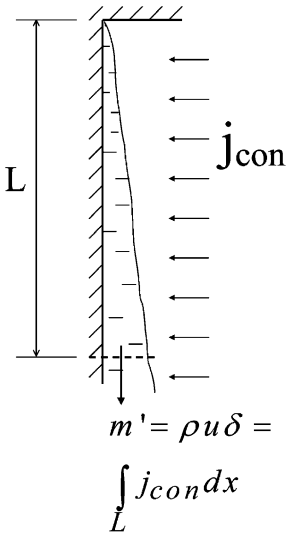

Fig. 2. Integration of condensing steam mass flux along the liquid film height.

Due to the small liquid film thickness, the actual position of the liquid film surface in Eq. (18) is approximated with the position of the pipe wall, i.e. $r = (R - \delta_1) \approx R$. Due to the applied finite control volume solution method and formulation of the source terms Γ_m for the condensation and absorption in the conservation equations (1)–(4), the suction of the steam due to the condensation is taken into account in the control volumes that lay on the pipe wall through the calculated pressure field. Hence, the steam flow towards the liquid film surface is not determined with the boundary velocity v_2 at $r = R$.

3.4. Absorption and degassing of non-condensables on the liquid film

The transport of non-condensables from the gas mixture to the liquid film (absorption) and vice versa (degassing) is a complex process that depends on the non-condensables concentrations in the gas mixture and liquid film, as well as on the liquid film temperature. In case of thick liquid films, the non-condensables concentration and transport by the liquid film is modelled with the conservation equation of the chemical spices concentration, where the concentration of non-condensables at the liquid film surface is saturated [27]. But, in case of the thin liquid film, it is possible to replace the time consuming solving of the multi-dimensional conservation equations in the form of partial differential equations with the algebraic closure laws.

It is shown here that for the thin liquid film flows, the gas concentration within the liquid film reaches saturation concentration at the short distance along the pipe. This means that the saturation condition of the non-condensables concentration within the whole thickness of the liquid film can be assumed, without taking into account the relaxation time of non-condensables transport from the liquid film surface to the liquid film inside layers or vice versa. The change of non-condensable $c = H_2,O_2$ mean mass fraction along the liquid film is determined with [27]

$$\frac{dg_{c,1}}{dx} = \frac{j_{a,c}}{\mu_1\delta_1\rho_1} = \frac{k_L(g_{c,1,j} - g_{c,1})}{u_1\delta_1} \tag{19}$$

where $(g_{c,1,i} - g_{c,1})$, represents a difference of the non-condensable mass fraction at the liquid film surface and its mean value within the liquid film. In Eq. (19) the absorption mass flux is calculated with

$$j_{a,c} = k_L\rho_1(g_{c,1,i} - g_{c,1}) \tag{20}$$

where the interface mass transfer coefficient is denoted as k_L. Introducing Eq. (16) in Eq. (19) and expressing the integral in Eq. (16) with its mean value it is obtained

$$\frac{dg_{c,1}}{dx} = \frac{k_L(g_{c,1,j} - g_{c,1})\rho_1}{j_{con}x} \tag{21}$$

Eq. (21) is integrated by assuming that the parameters $g_{c,1,i}$, k_L, ρ_1 and j_{con} are constant along the observed liquid film length. The following relation is obtained for the difference between non-condensables mass fraction at the liquid film surface and its mean value

$$\frac{g_{c,1,i}-g_{c,1}}{(g_{c,1,i}-g_{c,1})_{x0}}=\left(\frac{x}{x_0}\right)^{-\frac{k_L\rho_1}{j_{con}}} \tag{22}$$

From [27] it is estimated that $k_L \approx 10^{-5} \div 10^{-4}$ m/s. For low condensation heat fluxes the condensation mass flux is in the range $j_{con} \approx 10^{-5} \div 10^{-4}$ kg/m^{2}s. The values of k_L and j_{con} are of the same order of magnitude, and equation (22) shows that the mean non-condensable mass fraction in the liquid film reaches the saturation value along the very short liquid film path due to the high value of ρ_1 in the power on the r.h.s. of Eq. (22)

$$\frac{g_{c,1,i}-g_{c,1}}{(g_{c,1,i}-g_{c,1})_{x0}}\approx\left(\frac{x}{x_0}\right)^{-\rho_1}\rightarrow 0 \tag{23}$$

Therefore, the relaxation time of non-condensable gas transport within the liquid film can be neglected and the saturation concentration of non-condensables across the liquid film thickness can be assumed, i.e. $g_{c,1} \approx g_{c,1,i}$. This conclusion is utilised for the prediction of the absorption/degassing mass flux of non-condensables at the liquid film surface.

The mass conservation of non-condensables in the liquid film is

$$j_{a,c}=\frac{\partial(\delta_1\rho_1 g_{c,1})}{\partial t}+\frac{\partial(\delta_1\rho_1 v_1 g_{c,1})}{\partial x} \tag{24}$$

Since the relation $g_{c,1} \approx g_{c,1,i}$, holds, the mean non-condensables mass fraction at certain distance along the liquid film x is predicted from the empirical relation formulated in the form of Henry's law, which states that the molar fraction of absorbed gas at the liquid film surface $x_{c,1,i}$, is related to the non-condensable partial pressure in the gas mixture ρ_c

$$x_{c,1,i}=\frac{p_c}{H_c} \tag{25}$$

where H_c is the Henry's constant for the non-condensable c. By introducing the simple relation between non-condensable molar and mass fractions

$$x_{c,1,i}=g_{c,1}\frac{M_{1,i}}{M_c} \tag{26}$$

and the relation between the non-condensable mass fraction and partial pressure in the gas mixture

$$p_c=g_{c,2}p\frac{M_2}{M_c} \tag{27}$$

Eq. (25) is transformed in the following form:

$$g_{c,1}=g_{c,2}\frac{p}{H_c}\frac{M_2}{M_{1,i}} \tag{28}$$

where M denotes the molar mass.

Henry's constant H_{O_2} of oxygen in water is calculated with the correlation from [21]

$$\begin{aligned}H_{O_2}=\exp[&Q_1+Q_2p+Q_3p^2+(Q_4+Q_5p+Q_6p^2)T\\&+(Q_7+Q_8p+Q_9p^2)T^2\\&+(Q_{10}+Q_{11}p+Q_{12}p^2)\ln T]\end{aligned} \tag{29}$$

In Eq. (29) pressure p represents the partial pressure of oxygen in the gas mixture and it is expressed in bars. Temperature T is predicted as liquid film temperature, which is assumed to be equal to the steam saturation temperature determined by the steam partial pressure in the gas mixture, and it is expressed in (K). Coefficients in Eq. (29) are listed in Table 1. Calculated values of the Henry's constant are shown in Fig. 3 for pressures of 0.6 MPa and 7 MPa. Obviously, the Henry's constant is temperature dependent, while its dependence on pressure is weak. Data on the Henry's constant of hydrogen in water at elevated pressures and temperatures are not available in the open literature, while the relative difference of hydrogen to oxygen Henry's constant for water is approximately 10% at moderate pressures and temperatures [23]. Thus, the Henry's constant of hydrogen in water is assumed to be equal to that of oxygen, and it is determined also with Eq. (29).

Calculating the absorption mass flux with Eq. (24), the absorption rate is calculated as

$$\Gamma_{a,c}=j_{a,c}A_i/V_{CV} \tag{30}$$

where A_i is the interface surface within the control volume, while V_{CV} denotes a value of the numerical control volume.

3.5. Transient heat conduction in the pipe wall and insulator

Heat can be transferred from the mixture of non-condensables and steam to the pipewall by the mechanisms

Table 1
Coefficients in Eq. (29) for the calculation of Henry's constant of oxygen in water

Coeff.	Value	Coeff.	Value	Coeff.	Value	Coeff.	Value
Q_1	-2.10973×10^{2}	Q_4	-2.02733×10^{-1}	Q_7	9.77301×10^{-5}	Q_{10}	4.79875×10^{1}
Q_2	2.32745×10^{0}	Q_5	2.45925×10^{-3}	Q_8	-1.43857×10^{-6}	Q_{11}	-5.14296×10^{-1}
Q_3	-1.19186×10^{-2}	Q_6	-1.21107×10^{-5}	Q_9	6.84983×10^{-9}	Q_{12}	2.61610×10^{-3}

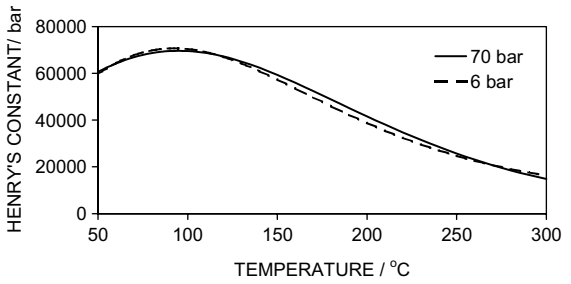

Fig. 3. Dependence of Henry's constant on pressure and temperature.

of steam condensation and convection or only by convection. Condensation exists if the local steam saturation temperature at the pipe wall (determined with the local steam partial pressure in the gas mixture) is higher than the inner pipe wall surface temperature. The inner pipe wall temperature and heat losses to the surrounding atmosphere are determined by the transient axial and radial heat conduction in the pipe's wall and insulator. In order to predict transient temperature field in the pipe's wall and insulator, a two-dimensional heat conduction equation is solved

$$\frac{\partial(\rho_k c_{p,k} T_k)}{\partial t} = \frac{1}{y^n}\frac{\partial}{\partial y}\left(y^n k_k \frac{\partial T_k}{\partial y}\right) + \frac{\partial}{\partial x}\left(k_k \frac{\partial T_k}{\partial x}\right) \tag{31}$$

where index 'k' denotes pipe wall (k = w) or pipe insulator (k = in). Pipe's wall and insulator parameters are: T, temperature; ρ, density; c_p, specific heat, and k is thermal conductivity. Parameter $n = 1$ holds for axisymmetric flow in a pipe (cylindrical coordinates), while $n = 0$ holds for plane flow (Cartesian coordinates).

Eq. (31) is solved for the prescribed boundary conditions. At the pipe wall top and bottom boundary, temperature is prescribed (symbols are depicted in Fig. 4)

$$\begin{aligned} T_w &= T_{w,T} \quad \text{at } x = x_T,\ y_{w1} < y < y_{w2} \\ T_w &= T_{w,B} \quad \text{at } x = x_B,\ y_{w1} < y < y_{w2} \end{aligned} \tag{32}$$

or the adiabatic conditions are applied

$$\frac{\partial T_w}{\partial x} = 0 \quad \text{at } (x = x_T \text{ or } x = x_B) \quad \text{and} \quad y_{w1} < y < y_{w2} \tag{33}$$

The insulator top and bottom boundaries are adiabatic

$$\frac{\partial T_{in}}{\partial x} = 0 \quad \text{at } (x = x_T \text{ or } x = x_B) \quad \text{and} \quad y_{w2} < y < y_{in} \tag{34}$$

The conduction and convection heat fluxes at the insulator outer surface are equal

$$k_{in}\frac{\partial T_{in}}{\partial y} = h_{atm}(T_{in} - T_{atm}) \quad \text{at } x_B < x < x_T,\ Y = Y_{in} \tag{35}$$

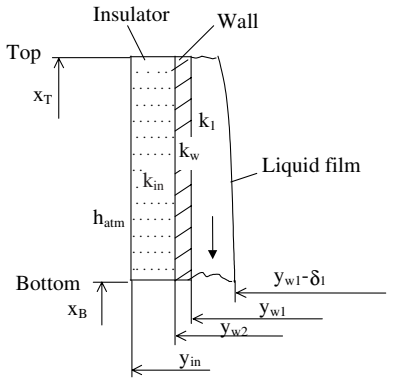

Fig. 4. Characteristic dimensions of the pipe wall and insulator.

where h_{atm} is the heat transfer coefficient due to convection from the insulator surface to the air atmosphere of temperature T_{atm}.

Pipe inner wall boundary condition, in case without steam condensation, is determined with the equality of the heat fluxes on the gas mixture and wall side

$$k_2\frac{\partial T_2}{\partial y} = k_w\frac{\partial T_w}{\partial y} \quad \text{at } x_B < x < x_T,\ y = y_{w1} \tag{36}$$

where k_2 is the thermal conductivity of the gas mixture at the wall surface, and T_2 is the gas mixture temperature. In case with the condensation on the wall inner surface, the wall inner surface temperature is equalised to the liquid film temperature in the control volume on the wall

$$T_w = T_1 \quad \text{at } x_B < x < x_T,\ y = y_{w1} \tag{37}$$

For the flow of the thin liquid film (several tens of microns, as it is the case for vertical non- vented pipes), the temperature drop across the liquid film thickness is neglected and the wall inner surface is equalised to the steam saturation temperature

$$T_w = T_{1,j} = T_{sat.}(p_{steam}) \quad \text{at } x_B < x < x_T,\ y = y_{wl} \tag{38}$$

The boundary condition stated with Eq. (38) neglects the temperature jump on the gas mixture–liquid film interface. This assumption is justified for atmospheric or higher pressures [28]. The steam partial pressure p_{steam} in Eq. (38) is determined with the Dalton's law

$$p_{steam} = p - p_{H2} - p_{O2} \tag{39}$$

and the partial pressures of hydrogen and oxygen are determined with Eq. (27). The mass fractions of non-condensables at the liquid film surface are the results of the solving of the conservation equations for non-condensables mass fraction, Eq. (7).

Since the thin liquid film resistance to heat transfer is neglected, the condensation rate (in cases when condensation exists) is determined with the heat conduction at the inner wall surface as

$$\Gamma_{\mathrm{con}} = k_{\mathrm{w}}\left(\frac{\partial T_{\mathrm{w}}}{\partial y}\right)_{y=y_{\mathrm{wl}}} A_{\mathrm{i}}/(\lambda V_{\mathrm{CV}}) \tag{40}$$

The possibility that a part of the pipe length is not covered with the insulator or that there is no insulator at all around the pipe wall is included in the model.

3.6. Calculation of gas mixture thermo-physical parameters

Density of the gas mixture is calculated as the sum of the component densities

$$\rho_2 = \rho_{\mathrm{steam}} + \rho_{\mathrm{O_2}} + \rho_{\mathrm{H_2}} \tag{41}$$

Steam density is calculated as a function of temperature and pressure with appropriate polynomials developed on the basis of steam tables [29]. Oxygen and hydrogen densities are calculated from the ideal gas law. Gas mixture and component densities are depicted for two pressures in Figs. 5 and 6, assuming that the steam is saturated, that the mixture components are in the thermal equilibrium, and that the mole ratio of hydrogen to oxygen is 2:1 (this mole ratio is determined by the radiolysis of the water molecules, as will be explained later on). The gas mixture density-temperature dependencies for the highest temperatures of 285.8 °C at 7 MPa and 158.8 °C at 0.6 MPa correspond to the negligible amount of hydrogen and oxygen in the mixture. With the non-condensables concentration increase, the steam partial pressure is decreased and the steam saturation (i.e. gas mixture) temperature is decreased. The mixture density curve has a minimum, for 0.6 MPa the minimum is located at approximately 95 °C and for 7 MPa at approximately 185 °C.

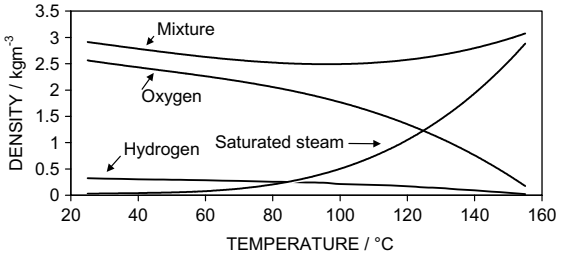

Fig. 5. Gas mixture and components densities at 0.6 MPa.

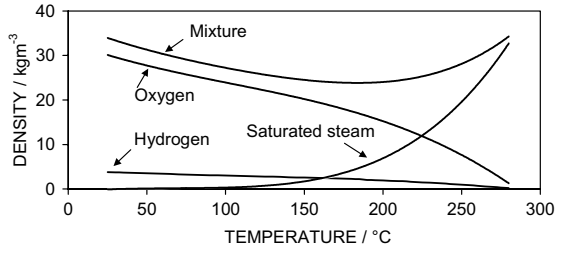

Fig. 6. Gas mixture and components densities at 7 MPa.

In the calculation of diffusion coefficients in the ternary steam–oxygen–hydrogen gas mixture, the appropriate coefficients of diffusion in binary mixtures are calculated first with the Gilliland relation [30]

$$D_{ij} = 435.7 \cdot 10^{-4} \frac{T_2^{3/2}}{p(V_i^{1/3} + V_j^{1/3})^2}\sqrt{\frac{1}{M_i} + \frac{1}{M_j}} \tag{42}$$

where V_i and V_j, are the molecular volumes of constituents i and j, Table 2. Diffusion coefficient D_{ij} is calculated in (m^2/s), gas mixture temperature T is expressed in (K), pressure p is the total gas mixture pressure in (Pa), and the molar weight M is expressed in (kg/k mole).

The diffusion coefficient of component c in a multi-component gas mixture (three or more components in the mixture), D_{c}, is calculated with the Wilky's formula [31]

$$D_c = \sum_{j\neq c} \frac{g_j}{M_j}\left(\frac{g_j}{M_j D_{jc}}\right)^{-1} \tag{43}$$

The specific heat of the multi-component gas mixture is calculated as [22]

$$c_{p,2} = \sum_{\mathrm{c}=1}^{m} g_{\mathrm{c}} c_{p,\mathrm{c}} \tag{44}$$

The dynamic viscosity μ_2 and thermal conductivity k_2 of the multi-component gas mixture are calculated as recommended by Bird et al. [22]

$$\mu_2 = \sum_{i=1}^{m} \frac{x_i \mu_i}{\sum_{j=1}^{n} x_k \Phi_{ij}} \tag{45}$$

and

$$k_2 = \sum_{i=1}^{m} \frac{x_i k_i}{\sum_{j=1}^{m} x_k \Phi_{ij}} \tag{46}$$

where

$$\Phi_{ij} = \frac{1}{\sqrt{8}}\left(1 + \frac{M_i}{M_j}\right)^{-1/2}\left[1 + \left(\frac{\mu_i}{\mu_j}\right)^{1/2}\left(\frac{M_j}{M_i}\right)^{1/4}\right]^2 \tag{47}$$

In Eqs. (44)–(46) m denotes the number of components that forms a gas mixture, and x is the molar fraction.

Table 2
Molecular volumes

Hydrogen, molecule (H_2)	14.3
Oxygen, molecule (O_2)	7.4
Water	18.8

4. Numerical solution procedure

The SIMPLE type [19] numerical algorithm is applied to the solution of governing partial differential equations (1)–(4), (7), (31). A discretization of these equations is carried out by their integration over control volumes of variable size in the two-dimensional Cartesian or cylindrical coordinate system. Non-condensables mass conservation equations, gas mixture energy conservation and pressure correction equation are integrated over scalar control volumes, while the gas mixture momentum conservation equations are integrated over staggered control volumes. The convective and diffusive terms at the control volume boundaries are determined with the power law numerical scheme as presented in [19]. Fully implicit time integration is applied. The pressure field is calculated according to the modified SIMPLE numerical method presented in [20], which takes into account the presence of two phases—liquid and gas. The resulting set of difference equations is solved with the Alternating Direction Implicit (ADI) method.

The iterative calculation procedure is performed as follows:

1. Gas mixture temperature field (Eq. (4)), pipe's wall and insulator temperature fields (Eq. (31)), non-condensables' mass fractions (Eq. (7)) and liquid film parameters Eqs. (14)–(17) are calculated for scalar control volumes.
2. Gas mixture velocity components are calculated for staggered control volumes (Eqs. (2) and (3)).
3. Pressure correction equation is solved for scalar control volumes (pressure correction equation is obtained by introducing the velocity components of gas mixture, expressed from momentum equations (2) and (3), and liquid film velocity from Eq. (14)–(16) into the mass conservation equation (1) [19,20]).
4. The velocity field is corrected with the corrected pressure values.
5. If the error of the mass balance in all scalar control volumes is not lower than the prescribed value and the number of outer iterations is lower than the prescribed integer, the program execution is returned to step 2. Otherwise, the program execution is continued with the next step.
6. If the error of the mass balance in all scalar control volumes is lower than the prescribed value, the program execution is continued with the next step, otherwise the time step is divided by two, the current values of dependent variables are equalised to the initial ones and the program execution is returned to step 1.
7. The time is increased, new values of dependent variables are assigned to initial ones for the new time step of integration and the physical properties are updated with the new values of the dependant variables.
8. If the end of the transient is reached the program execution is stopped, otherwise the program execution continues with step 1.

The convergence of the numerical procedure is achieved by performing the calculation within the prescribed errors for inner and outer iterations. The set of algebraic equations obtained by the discretization of one conservation equation is solved within the inner iterations. The inner iterations are performed until the maximal difference of calculated dependent variable in two consecutive iterations in all control volumes is not less than prescribed error. This criterion is satisfied in the calculation of all variables. The outer iterations are applied to the solving of all sets of discretized governing equations. By the solving of pressure correction equation, the maximum error of mass balance for all scalar control volumes is determined. The outer iterations are performed until the maximum mass balance error is not lower than the prescribed error. If this criterion can not be satisfied for certain acceptable number of outer iterations, the time step of integration is reduced by two and the solution procedure is repeated as described in previous section.

The stability of the numerical procedure is satisfied by calculating the time step of integration according to the Courant criterion

$$\Delta t < \min\left(\frac{\Delta x}{u}, \frac{\Delta y}{v}\right)_{i,j} \tag{48}$$

where i and j denotes counters of the control volumes. Both gas mixture and liquid film velocities are considered in Eq. (48). Although the implicit time integration method is applied, the restriction of Eq. (48) that the fluid particle propagates only within the control volume in one time step of integration is imposed in order to track the non-condensables concentration front. Numerical simulations showed that even one-tenth of the time step calculated with the r.h.s. of Eq. (48) must be applied in order to preserve required accuracy in transients with large concentration differences. The transient heat conduction is less restrictive regarding the stability and accuracy of numerical calculation.

5. Verification, results and discussion of the proposed modelling approach

5.1. Steam-air flow over a vertical plate

As a part of the verification of the developed model and applied numerical method, a prediction of the heat transfer coefficient for the condensation on a flat plate in the presence of a non-condensable is performed. The downward external flow of steam–air mixture is

observed over the uniformly cooled vertical plate (Fig. 7—obtained by the numerical simulation and represents the flow conditions). A boundary layer flow of steam–air mixture is formed over the liquid film. The grid refinement tests show that grid independent results are obtained for the length of the control volume of 0.2 m in the stream wise direction and with 50 control volumes within the width of 0.3 m, where the control volume width is gradually decreasing towards the plate, as shown in Fig. 8. A flow of steam-air mixture with uniform velocity is directed towards a vertical plate at the plane $x = 0$ m in Fig. 7. On the left boundary of the flow domain, which is on a sufficient distance from the vertical plate to completely comprise velocity, temperature and non-condensable concentration boundary layers (at $y = 0$ m in Figs. 7 and 8), the velocity boundary conditions are

$$\frac{\partial u_2}{\partial y} = 0 \quad \text{and} \quad v_2 = 0 \tag{49}$$

At the flow domain outlet at $x = 2$ m in Figs. 7 and 8, the velocity boundary conditions are

$$\frac{\partial u_2}{\partial y} = 0 \quad \text{and} \quad \frac{\partial v_2}{\partial y} = 0 \tag{50}$$

The liquid film drains on the plate due to the steam condensation. The liquid film velocity and thickness are determined with Eqs. (14)–(17), and the gas mixture boundary velocities at the liquid film surface with Eq. (18). Gas mixture temperature and air mass fraction are specified at $x = 0$ m, while at the outlet $x = 2$ m and far from the plate at $y = 0$ m it holds

$$\frac{\partial T_2}{\partial n} = 0 \quad \text{and} \quad \frac{\partial g_2}{\partial n} = 0 \tag{51}$$

where n is the co-ordinate normal to the boundary plane. The condensation takes place in the control volumes that lay on the vertical plate (as it was already stated, the liquid film is thin and it is whole comprised in the control volumes that lay on the wall), so, the gas mixture temperature in these control volumes is equal to the steam saturation temperature determined by the local steam partial pressure. The adiabatic condition as given with Eq. (51) is applied for the air mass fraction at the plate wall. The plate is cooled with the constant heat flux of 500 W m^{-2}. The total inlet steam air pressure is 0.1 MPa. The air thermo-physical parameters are prescribed according to [22,23].

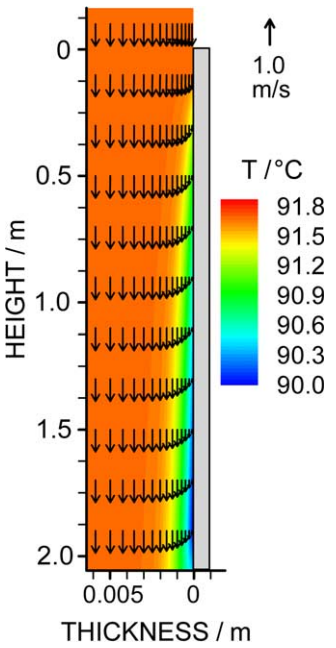

Fig. 7. Velocity and temperature fields in two-dimensional plane flow of steam and air mixture over vertical plate (air mass fraction of 0.4).

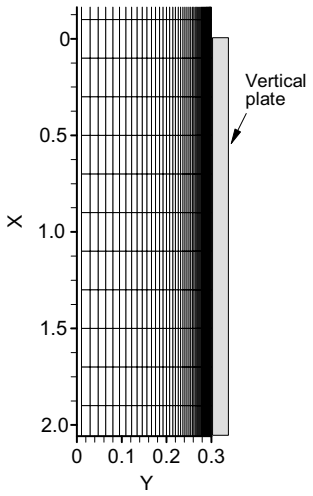

Fig. 8. Numerical grid with 30×50 control volumes in x–y directions for the simulation of external steam–air flow over uniformly cooled vertical plate (10 upstream and 9 downstream rows of control volumes are not shown for the sake of more detailed presentation in the plate region).

Due to the condensation in the presence of non-condensable air, the air concentration near the liquid film surface is increased, the steam partial pressure is decreased and, consequently, the saturation temperature of condensing steam is decreased. The results of the numerical simulation in Fig. 7 clearly show the formation of the velocity and temperature boundary layers on the vertical plate. Numerically predicted mean heat transfer coefficients for 2 m long plate are compared with the predictions of engineering correlations of Uchida [7], Tagami [8], and MIT correlation [9] for the range of air mass fractions from 0.1 to 0.9, Fig. 9. The mean heat transfer coefficient is calculated as

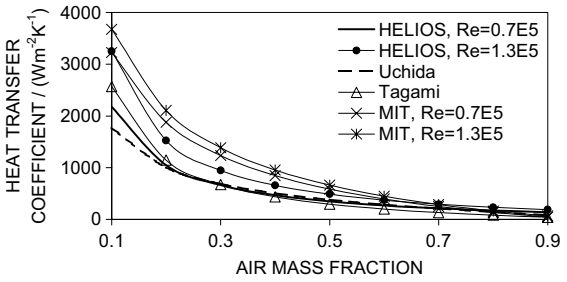

Fig. 9. Comparison of the condensation heat transfer coefficient of steam in the presence of air calculated with the HELIO code and engineering correlations.

$$\bar{h} = \frac{1}{L}\int_L h\,\mathrm{d}x \tag{52}$$

where L represents plate length. The characteristic dimension in the definition of the Reynolds number depicted in Fig. 9 is the vertical plate length L, thus $Re = U_\infty L/v$. Fig. 9 shows that the numerically predicted results are dependent on the Reynolds number. Good agreement is obtained with the Uchida and Tagami correlations for the Reynolds number of 0.7×10^4. The MIT correlation gives higher values for air mass fractions lower than 0.8, which can be attributed to the fact that the MIT correlation is developed for the turbulent flow over the vertical plate, characterised with the Reynolds numbers higher than approximately 5×10^5 [23] (obviously the numerical results presented in Fig. 9 are obtained for the laminar flow regimes for Reynolds numbers of 0.7×10^4 and 1.3×10^4).

The results presented in Figs. 7 and 9 are obtained with the mass balance error for each control volume less than 10^{-10} kgs^{-1}.

5.2. Dynamics of hydrogen and oxygen accumulation in a vertical non-vented pipe

A vertical pipe 2 m long and with an inner diameter of 0.03 m is open at the bottom and closed at the top, Fig. 10. The pipe wall thickness is 0.003 m, and its insulation thickness is 0.02 m. The pipe wall parameters are: thermal conductivity $15\,\mathrm{W\,m^{-1}\,K^{-1}}$, specific heat $500\,\mathrm{J\,kg^{-1}\,K^{-1}}$ and density $8000\,\mathrm{kg\,m^{-3}}$. The insulator parameters are: thermal conductivity of $0.05\,\mathrm{W\,m^{-1}\,K^{-1}}$, specific heat $800\,\mathrm{J\,kg^{-1}\,K^{-1}}$ and density $300\,\mathrm{kg\,m^{-3}}$. The coefficient of heat transfer from the insulator outer surface to the ambient air of 40 °C is $5\,\mathrm{W\,m^{-2}\,K^{-1}}$. Initially, the pipe is filled with the gas mixture of saturated steam and a small amount of hydrogen and oxygen with the mass fractions of 2.5×10^{-3} and 20.0×10^{-3}, respectively. The total gas mixture pressure is 7 MPa. The pipe is connected at the bottom with a large volume filled with the steam–hydrogen–oxygen mixture at the same

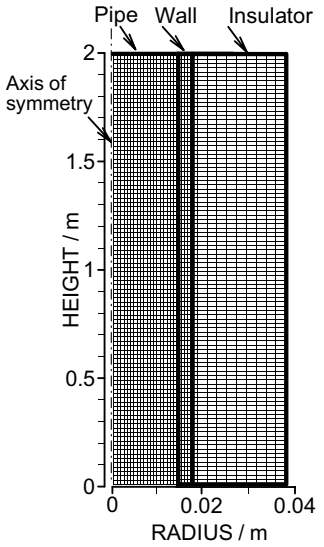

Fig. 10. Numerical grid with 100×20 control volumes inside pipe, 100×5 in pipe wall and 100×10 in insulator.

pressure. The mass fractions of hydrogen and oxygen at this boundary are constant and equal to the initial mass fractions in the vertical pipe.

The grid refinement tests have shown that practically grid independent results are obtained for 100×20 control volumes inside pipe in (height × width) directions respectively, 100×5 control volumes in the pipe wall, and 100×10 in the insulator. The following boundary conditions are applied. Components of the gas mixture velocity are zero at the pipe top, at the pipe axis of symmetry the velocity boundary condition is given with Eq. (49), for the pipe bottom Eq. (50) is applied. Due to the heat losses to the surrounding the condensation occurs and the water film drains along the inner pipe wall. The liquid film and gas mixture parameters in the control volumes that lay on the pipewall are determined as in the test case presented in the previous Section 5.1. Gas mixture temperature and air mass fraction are specified for the inlet gas mixture flow at the pipe bottom, while for the axis of symmetry and for the pipe closed top end Eq. (51) holds. Pipe wall and insulator boundary conditions are described in Section 3.5. Pipewall temperature at the bottom end is equal to the gas mixture inlet temperature, while the pipe top end is adiabatically insulated. Both insulator ends in axial direction are adiabatically insulated. In order to avoid counter-current gas mixture and liquid film flow at the pipe open bottom end, which leads to calculation instability and substantial increase of the calculation errors of the velocity field, it is assumed that the pipe is adiabatically insulated 0.3 m from the bottom and the whole liquid film flow is removed in the control volume at the

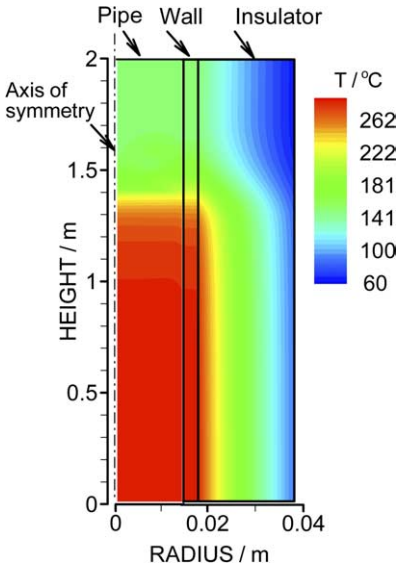

Fig. 11. Temperature field in the gas mixture, pipe wall and insulator of the vertical non-vented pipe open at the bottom and closed at the top after 2.78 h of accumulation.

location of 0.3 m from the pipe bottom. These boundary conditions enable stable and accurate numerical transient simulation, without the influence on the dynamics of the hydrogen–oxygen accumulation within the pipe.

Fig. 11 shows the temperature field in the gas mixture, pipe wall and insulator, as the result of the transient calculation of conjugate heat transfer in the gas mixture and solid walls. The temperature fields are coupled and show both radial and axial heat conduction. Due to the hydrogen–oxygen accumulation from the pipe top, a zone of lower temperature is formed from the pipe top down to the height of approximately 1.35 m. The corresponding hydrogen and oxygen mass fraction and gas mixture temperature fields are compared in Fig. 12. It is shown that these fields are strongly coupled. The temperature front is located at the same level as accumulated non-condensables front. The ratio of accumulated hydrogen to oxygen mass fraction is shown in Fig. 13. Approximately constant value of 0.125 is obtained, which correspond to the initial and boundary hydrogen to oxygen mole ratio of 2:1. This ratio is determined by the process of water molecule radiolyses—the H_2O molecule is separated into H_2 and O, where oxygen atoms are recombined into O_2 molecules, and the process results into 2:1 mole ratio. Corresponding mass fractions are calculated as follows. The hydrogen mass fraction is

$$g_{H_2} = \frac{M_{H_2} x_{H_2}}{M_{H_2} x_{H_2} + M_{O_2} x_{O_2} + M_{H_2O} x_{H_2O}} \tag{53}$$

The oxygen mass fraction is

$$g_{O_2} = \frac{M_{O_2} x_{O_2}}{M_{H_2} x_{H_2} + M_{O_2} x_{O_2} + M_{H_2O} x_{H_2O}} \tag{54}$$

Dividing Eq. (54) with Eq. (53) and introducing 2:1 mole ratio of hydrogen to oxygen as

$$\frac{x_{H_2}}{x_{O_2}} = 2 \tag{55}$$

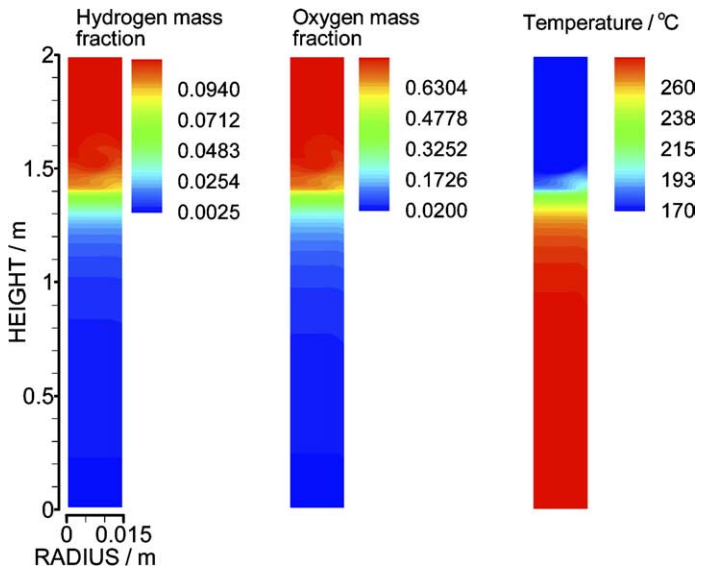

Fig. 12. Hydrogen and oxygen mass fractions and gas mixture temperature after 2.78 h of accumulation.

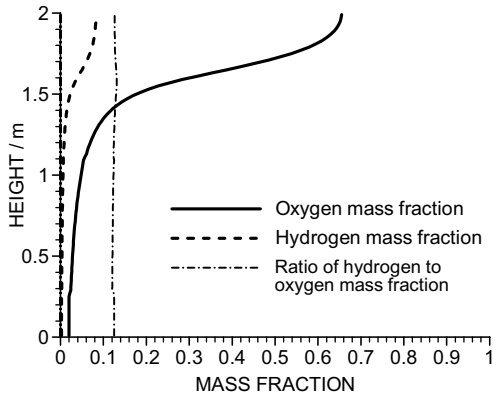

Fig. 13. Hydrogen and oxygen mass fraction profiles along the pipe centerline after 2.78 h of accumulation.

and the molar weights of hydrogen $M_{H_2} = 2\,\mathrm{kg\,kmol^{-1}}$, oxygen $M_{O_2} = 32\,\mathrm{kg\,kmol^{-1}}$ and steam $M_{H_2O} = 18\,\mathrm{kg\,kmol^{-1}}$, the ratio of hydrogen to oxygen mass fractions is obtained as

$$\frac{g_{H_2}}{g_{O_2}} = 0.125 \tag{56}$$

which is the same value as the results of the complex numerical prediction depicted in Fig. 13. In the experimental investigation of the non-condensables accumulation in the long complex pipeline, performed within the investigation of the nuclear power plant incident [1], it was showed that the initial and boundary mole ratio 2:1 of non-condensable gases is preserved during the transient in all points of the experimental pipe. Here presented numerical results verifies that the developed HELIO code is able to predict the right mole ratio of radiolytic gases during the long duration of transient, and within the whole calculation domain with intensive changes of radiolytic gases concentrations.

Fig. 14 shows a typical gas mixture velocity field in the pipe during the non-condensables accumulation. The shear stress at the liquid film surface causes the downward gas mixture flow in the vicinity of the wall. The condensing steam is being replenished with the inlet gas mixture flow from the open pipe bottom. As the steam is being condensed on the wall, the intensity of the gas mixture velocity is reduced along the pipe.

Fig. 15 shows the results of the grid refinement tests. The numerical results do not depend on the grid in the initial period of the transient (as it is shown by temperature profiles after 1.39 h). But the dependence on the grid refinement is more and more pronounced as the volume of the accumulated non-condensables is increased (the strongest dependence of the calculated temperature profile on the grid refinement is observed after 4.44 h

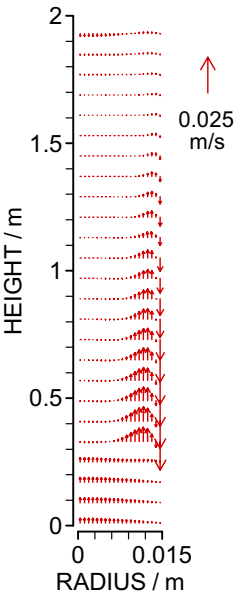

Fig. 14. Gas mixture velocity field in the vertical pipe closed at the top and open at the bottom after 1.39 h of the non-condensables accumulation due to the condensation.

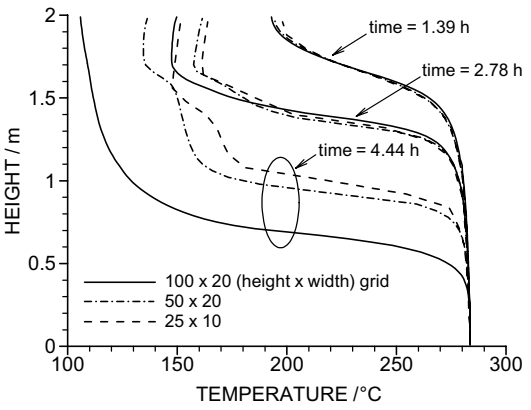

Fig. 15. Temperature profiles along the pipe centerline calculated with different numerical grids.

when the concentration front reaches the level of approximately 0.5 m).

The stronger dependence of the calculated temperature fields on the grid refinement in the later periods of the transient is caused by the formation of vortexes in the zone of concentration front and within the volume of accumulated non-condensables, Fig. 16. One vortex exists at the top of the pipe during the initial period of the hydrogen–oxygen accumulation, Fig. 16a. Two vortexes with opposite directions of rotation are

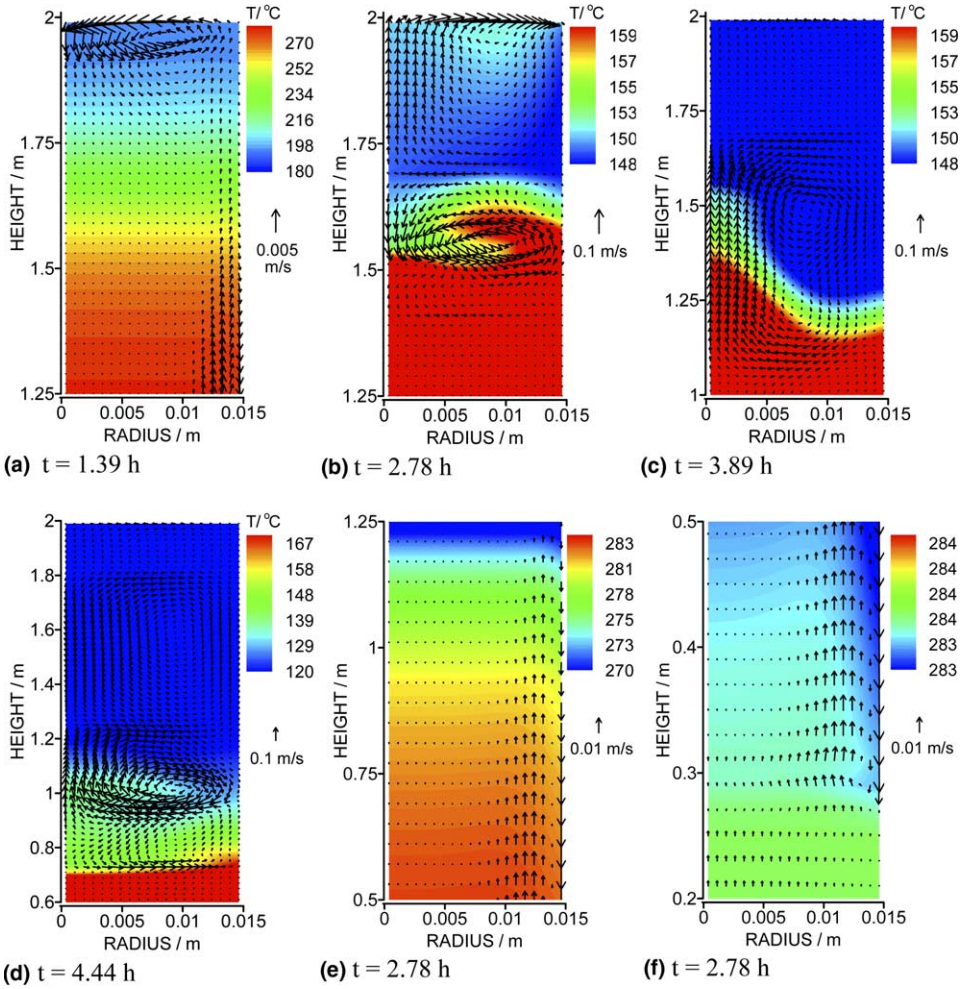

Fig. 16. Temperature and velocity fields in the vertical non-vented pipe at several instants during the non-condensables accumulation transient and at different elevations.

formed in the later period of the transient, one at the top of the pipe and the other across the front of non-condensables concentration, Fig. 16b. Further, the vortex across the concentration front is enlarged, Fig. 16c. During the last period of the transient a complex flow structure is formed across the concentration front and within the volume of accumulated non-condensables, Fig. 16d. Below the concentration front, the gas mixture flow at the immediate vicinity of the wall is directed downwards due to the shear with the draining liquid film, while further from the wall the gas mixture flows upwards and replenishes the condensing steam, Fig. 16e. Near the pipe bottom the recirculation of the descending gas mixture occurs, Fig. 16f. The presented flow structures are the result of three effects: the shear of the gas mixture and liquid film, the suction of the steam from the gas mixture due to the condensation on the liquid film surface and its replenishment with the inlet gas mixture, and the convection due to the buoyancy forces induced by the gas mixture density variations within the flow field. The density differences and corresponding buoyancy forces are caused by the non-uniformity of the hydrogen and oxygen concentrations and temperature fields. It was already shown in Fig. 6 that the mixture temperature decrease (from its initial value that corresponds to the state with low concentration of non-condensables) leads first to the decrease of the gas mixture density, and after passing through the minimum, to the increase of the density. It should be stated that the calculated temperature field is close to the steam saturation temperature field determined with the steam partial pressure field (differences between local calculated gas mixture temperatures and steam saturated temperatures are lower than 1 °C). This means

that the relation given in Fig. 6 can be applied to the analyses of here obtained results. The buoyancy forces have the domain influence on the formation of vortexes within the accumulated non-condensable volume and across the non-condensables front (Fig. 16a–d). Temperature field presented in Fig. 16a is in the range between 180 °C and 270 °C. In this range the gas–mixture concentration increase and temperature decrease, as presented in Fig. 6. Since the non-condensables concentration is higher and the temperature is lower near the pipe wall due to the condensation (Fig. 16a), the gas mixture density is lower near the wall, and the gas mixture ascends along the cooled wall and the vortex is formed at the pipe top. The temperature fields in Fig. 16b–d are in the range below 185 °C, which means according to Fig. 6, that the gas mixture density increases with the non-condensables concentration increase and temperature decrease. Hence, the induced buoyancy forces lead to ascending flows in the higher temperatures areas (due to lower densities), and to descending flows in lower temperature areas (where density is higher).This circulation direction is clearly demonstrated in the areas of non-condensables concentration fronts in Fig. 16b and c. The vortexes across the concentration front and within the accumulated volume in Fig. 16b and c rotate in opposite directions. Also, these directions of rotation changes during the transient, in Fig. 16b gas mixture ascends along the wall at the non-condensable front location, while in Fig. 16c gas mixture descends at this location. This behaviour leads to complex flow structure in the later period of the transient when the volume of accumulated non-condensables is enlarged, as presented in Fig. 16d.

Liquid film parameters are shown in Fig. 17. Liquid film mass flow rate is increasing from the pipe top due to condensation, Fig. 17a, except at the location of the non-condensables concentration front between 1.38 m and 1.5 m (this concentration front is shown in Fig. 16b which corresponds to the same time instant). At the stated location the wall inner surface temperature is higher than the steam saturation temperature determined with the steam partial pressure, which means that the condensation is stopped at this short distance. The liquid film thickness and velocity are gradually increasing from the pipe top, with a certain disturbance at the location of the concentration front (Fig. 17b and c). Fig. 17d shows the mass flux of absorbing oxygen at the liquid film surface. The absorption is practically stopped below the condensation front since the hydrogen and oxygen mass fractions are much lower in this region (close to the inlet boundary value of 22.5×10^{-3}) than mass fractions in the volume of accumulated non-condensables above the concentration front (which is located at approximately 1.5 m).

The results presented in this Section are obtained with the mass balance error of 10^{-9} kgs^{-1} for every control volume. The calculation of 4.5 h transient with 100×20 control volume lasts approximately 200 h on a PC computer with 1.7 GHz processor.

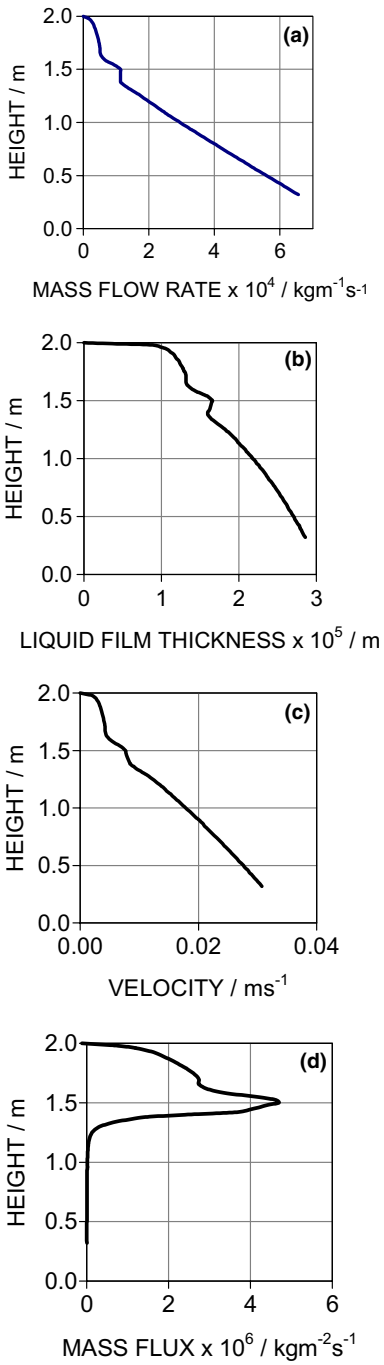

Fig. 17. Liquid film parameters after 2.78 h of non-condensables accumulation (from top to bottom: liquid film mass flow rate, liquid film thickness, velocity and oxygen absorption mass flux at the liquid film surface).

5.3. Simulation of radiolytic gasses accumulation in a long pipe of a nuclear power plant auxiliary system

A temperature decrease at the top of a vertical pipe due to the radiolytic gases hydrogen and oxygen accumulation was recorded at an auxiliary system of the nuclear power plant and reported in [3]. The pipe was 16 m long and its inner diameter was 0.34 m. The pipe top was closed, while the bottom was opened and connected to the rest of the system at the total pressure of 0.6 MPa. The pipe wall thickness was 0.008 m. It is estimated that the pipe was without insulator 2 m from the top, while the rest of the pipe had an insulator of 0.08 m thickness. The thermo-physical parameters of the pipe wall were as follows: thermal conductivity $15\,W\,m^{-1}\,K^{-1}$, specific heat $500\,J\,kg^{-1}\,K^{-1}$, and density $8000\,kg\,m^{-3}$. Insulator parameters were: thermal conductivity $0.042\,W\,m^{-1}\,K^{-1}$, specific heat $800\,J\,kg^{-1}\,K^{-1}$, and density $300\,kg\,m^{-3}$. The initial mass fractions of hydrogen and oxygen were 2.5×10^{-6} and 20.0×10^{-6}, respectively. The temperature was measured with a thermocouple placed on the non-insulated outside wall of the pipe 0.05 m from the pipe top.

The half of the pipe geometry from the axis of symmetry to the outside surface of the insulator is modelled in cylindrical co-ordinates. Applied numerical grid consists of 100×10 control volumes inside pipe in axial and radial direction, 100×4 control volumes in the pipe wall, and 100×4 control volumes in the insulator. The control volumes are equally spaced in radial direction inside pipe, in the wall and insulator, but non-uniform grid is applied in axial direction, Fig. 18, in order to minimise the required computer calculation time. The entrance length of 2 m from the pipe bottom is discretized with 10 uniform control volumes in axial direction (Fig. 18), then 30 control volumes with gradually increasing length are placed within next 10.75 m, 30 control volumes with gradually decreasing length are placed in next 4.75 m, and the last 0.5 are modelled with equally spaced 30 control volumes. The finest grid is applied at the pipe top with the aim to calculate the hydrogen and oxygen accumulation in the short distance from the pipe top and to reduce the concentration and temperature front smearing in this zone. The number of control volumes was not further increased, since the simulated transient time period is long (40 days), and further substantial increment of control volumes would require very long computational times, which would not be justified by the accuracy of obtained results. The applied boundary conditions are the same as in the previous calculation presented in Section 5.2.

Also, in order to reduce the long computational time, the simulations are performed with 50, 300 and 1000 times higher initial and boundary mass fraction of non-condensables than the real value of 22.5×10^{-6} at the plant. The calculated simulation time is linearly increased according to the increase of the initial mass fraction, and the obtained results are shown in Fig. 19 (for instance, 50 times increment of initial and boundary mass fraction of hydrogen and oxygen is also accompanied with 50 times increment of the simulation time, this also mean that the required computational time is reduced approximately 50 times). It is shown that the results obtained for 50 times higher non-condensables initial/boundary mass fractions give the closest agreement with the measured data, while the results obtained with 300 times and 1000 times higher mass fractions overpredict the measured data. The reason that the linear time scale cannot be applied is the non-linear behaviour of the gas mixture convection. Velocity fields in cases of 50 and 1000 times increased initial/boundary mass fractions are shown in Figs. 20 and 21 respectively. In case of 50 times initial/boundary mass fractions increase, the recirculating flow is formed, with ascending

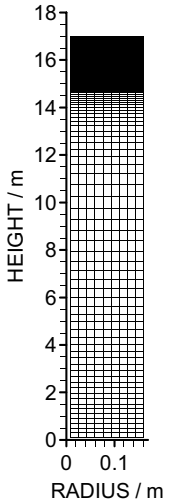

Fig. 18. Numerical grid for the simulation of radiolytic gases accumulation at the Nuclear Power Plant.

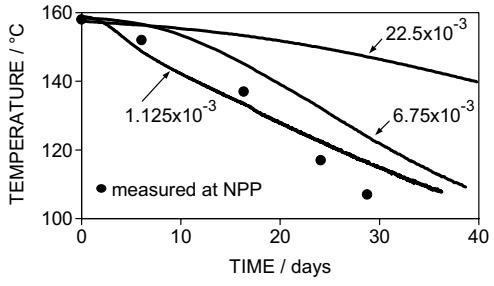

Fig. 19. Comparison of measured and calculated data. Calculations are performed for different initial and boundary mass fractions of radiolytic gases, time is linearly scaled with the mass fraction.

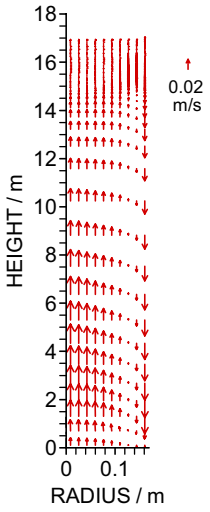

Fig. 20. Velocity profile for the initial/boundary mass fraction of radiolytic gases equal to 1.125×10^{-3}.

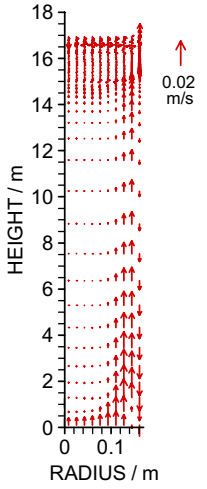

Fig. 21. Velocity profile for the initial/boundary mass fraction of radiolytic gases equal to 22.5×10^{-3}.

flow in the pipe core and descending flow at the pipe wall. Descending flow at the pipe wall is the result of the gas mixture–liquid film shear. In case of 1000 times non-condensables initial/boundary mass fraction increment the ascending gas mixture flow is moved towards the pipe wall, while in the pipe core the mixture is nearly stagnant. Such behaviour is the result of more intensive change of gas mixture density near the wall, and corresponding more intensive buoyancy forces in this zone than in the case of 50 times initial/boundary non-condensables mass fraction increase. Hence, the results in Fig. 19 show that up to 50 times increment of initial and boundary non-condensables mass fraction is acceptable with the aim to reduce the necessary computational time. Since the measured data in Fig. 19 were obtained for the long time period at the plant (during which same of the ambient or boundary conditions could be changed—details about the ambient and other boundary conditions were not recorded at the plant), and with the accuracy of the industrial measurement, the agreement between calculated and measured temperatures is acceptable.

The calculation of the results presented in Fig. 19 for 1.125×10^{-3} initial mass fraction of non-condensables is performed with the mass balance error of $10^{-9}\,\mathrm{kg\,s^{-1}}$ for every control volume. The calculation of the 38 h transient lasts approximately 90 h on a PC computer with 1.7 GHz processor.

6. Conclusion

A complex thermal–hydraulic and physico-chemical two-dimensional model is presented for the prediction of hydrogen and oxygen accumulation induced by the steam condensation in the vertical non-vented pipe. The mass, momentum and energy balance equations are stated for the gas mixture flow by taking into account that two phases exist near the pipe's wall due to liquid film drainage. Hydrogen and oxygen convection and diffusion in the mixture with steam are described with the mass fraction conservation equations, which are written for each non-condensable. In order to improve the efficiency of the developed method and to reduce time consuming computations of long transient accumulation processes, the condensate liquid film flow is modelled according to the Nusselt theory. The applied shear free boundary conditions at the liquid film surface are justified for the conditions of natural convection in the pipe during non-condensables accumulation. The saturated concentration of non-condensables in the thin liquid film is justified and the mass absorption rate of non-condensables is predicted by solving the mass fraction conservation equation for the liquid film and by applying the Henry's law. Transient radial and axial heat conduction in the pipe's wall and insulator is predicted with the two-dimensional Fourier's equation. Compound boundary conditions are presented for stated thermal–hydraulic and physico-chemical conditions. Calculation of the gas mixture thermo-physical parameters is described. The presented model is applied to the prediction of heat transfer coefficient for the condensation in the presence of non-condensables, to the detailed investigation of the hydrogen and oxygen accumulation in the vertical pipe closed at the top and opened at the bottom, and to the simulation of the nuclear power plant conditions of hydrogen and oxygen accumulation in the long vertical pipe. The major findings are as follows.

(a) The hydrogen and oxygen accumulation is initiated at the pipe top. The concentration front of accumulated non-condensables is formed and propagates downwards from the pipe top. The non-condensables concentration and gas mixture temperature fields, as well as concentration and temperature fronts are strongly coupled.
(b) The gas mixture convection in the pipe is determined with the wall liquid film–gas mixture shear, with the steam suction due to the condensation at the liquid film surface and replenishment of the condensed steam with the inlet gas mixture at the pipe open bottom, and with the buoyancy forces caused by the non-uniform non-condensables concentration fields and gas mixture temperature field.
(c) Due to the low liquid film thickness on the inside wall of the non-vented insulated pipe that is cooled by natural convection of the ambient air, and due to the low gas mixture velocities under the conditions of natural convection induced by non-condensables concentration and temperature non-uniform fields, the Nusselt approach can be applied to the liquid film flow modelling. The liquid film drainage on the wall influences the gas mixture velocity field through the shear on the liquid film surface.
(d) At the nuclear power plant the mass fractions of radiolytic hydrogen and oxygen in the mixture with steam are very low 22.5×10^{-6}. The simulation of hydrogen and oxygen accumulation in non-vented pipe with this initial mass fraction value requires substantial computational time. The sensitivity analyses have shown that computational procedure can be speeded up with an increase of the initial and boundary non-condensables mass fractions approximately up to 50 times, where the simulation time can also be increased for fifty times and the computational (computer) time can be reduced approximately 50 times. Further increase of non-condensables mass fraction will lead to difference of the gas mixture velocity field and a linear increase of the simulation time in the same proportion as the increase of the initial and boundary non-condensables mass fractions is not preserved.
(e) Besides the non-condensables initial and boundary mass fractions, the pipe diameter determines the accumulation time. In Section 5.2 it is shown that the hydrogen and oxygen accumulation in 2 m long pipe with a diameter of 0.03 m lasts for approximately 4.5 h, while in case of 16 m long pipe with 0.34 m diameter the accumulation within the 0.05 m from the pipe top lasts approximately 38 days. Also, the reduction of the heat losses to the environment would reduce the rate of non-condensables accumulation.

The obtained results show that the developed method is able to efficiently predict hydrogen and oxygen accumulation due to the condensation in the vertical non-vented steam pipe during the long time periods of several days, weeks or even months. Further work on the application of the developed methodology will be directed towards the simulation of the non-condensables accumulation in the vertical pipe open at the top and with a pipe bottom submerged in the water pool (the conditions important for the blow-down pipe in the nuclear power plants with the Boiling Water Reactor and with a wet containment). Also, the case of interest is the accumulation in a non-vented vertical pipe closed at the top and connected at the bottom with a horizontal pipe in which the flow of the main steam exists. Three-dimensional cases of non-condensables accumulation in slightly inclined, inclined and complex steam pipelines are also under investigation.

References

[1] T. Narabayashi, Y. Yamamoto, T. Yamamoto, N. Ichikawa, A. Sudo, R. Matsukawa, Study on thermal–hydraulic accumulation mechanisms of non-condensable gases, in: JSME/ASME Proceedings of the Eleventh International Conference on Nuclear Engineering, Tokyo, Japan, 2003, Paper ICONE11-36510.
[2] U. Stoll, Hydrogen accumulation/combustion; lessons learned in various countries, example of Brunsbuettel in Germany, Invited Lecture for the Panel Session Hydrogen Accumulation/Combustion—Lessons Learned in Various Countries, The Eleventh International Conference on Nuclear Engineering, Tokyo, Japan, 2003.
[3] T. Diesselhorst, Accumulation of radiolytic gases in BWR steam piping and components, in: JSME/ASME Proceedings of the Eleventh International Conference on Nuclear Engineering, Tokyo, Japan, 2003, Paper ICONE11-36558.
[4] V. Gerasimov, A. Monakhov, Nuclear Engineering Materials, First ed., Mir Publisher, Moscow, 1983, pp. 98, 167–170.
[5] V. Stevanovic, Z. Stosic, U. Stoll, Condensation induced hydrogen accumulation on a non-vented pipe, in: JSME/ASME Proceedings of the Eleventh International Conference on Nuclear Engineering, Tokyo, Japan, 2003, Paper ICONE11-36384.
[6] V. Stevanovic, Z. Stosic, U. Stoll, HELIOS code simulation of condensation induced hydrogen accumulation in slightly inclined non-vented pipe, ASME Proceedings of the Twelfth International Conference on Nuclear Engineering, Washington D.C., 2004, paper ICONE12-49534.
[7] H. Uchida, A. Oyama, Y. Togo, Evaluation of post accident cooling system of light water power reactors, in: Proceedings of International Conference on Peaceful Uses of Atomic Energy, vol. 13, 1965, pp. 93 (quoted in [12]).
[8] Tagami, Interim report on safety assessments and facilities establishment project for June 1965, Japanese Atomic Energy, vol. 1, 1965 (quoted in [12]).

[9] A.A. Dehbi, M.W. Golay, M.S. Kazimi, The effects of noncondensable gases on steam condensation under turbulent natural conditions, Report MIT-ANP-TR-004,1991.
[10] E.M. Sparrow, W.J. Minkowycz, M. Saddy, Forced convection condensation in the presence of noncondensables and interfacial resistance, Int. J. Heat Mass Transfer 10 (1967) 1829–1845.
[11] C.Y. Wang, C.J. Tu, Effects of non-condensable gas on laminar film condensation in a vertical tube, Int. J. Heat Mass Transfer 31 (11) (1988) 2339–2345.
[12] N. Agoudjil, Numerical modelling of heat and mass transfer during condensation of steam containing noncondensable gas, in: Proceedings of the Ninth International Conf. on Numerical Methods in Thermal Problems, Atlanta, 1995, pp. 112–123.
[13] J.L. Munoz-Cobo, L. Herranz, J. Sancho, I. Tkachenko, G. Verdu, Turbulent vapour condensation with noncondensable gases in vertical tubes, Int. J. Heat Mass Transfer 39 (15) (1996) 3249–3260.
[14] V. Srzic, H.M. Soliman, S.J. Ormiston, Analysis of laminar mixed-convection condensation on isothermal plates using the full boundary-layer equations: mixtures of a vapour and a lighter gas, Int. J. Heat Mass Transfer 42 (1999) 685–695.
[15] C. Zhang, A. Bokil, A quasi-three-dimensional approach to simulate the two-phase fluid flow and heat transfer in condensers, Int. J. Heat Mass Transfer 40 (15) (1997) 3537–3546.
[16] N. Agoudjil, G. Avakian, Condensation of steam containing non-condensable gas on a single horizontal tube and a tube bank, in: G.P. Celata, P. Di Marco, A. Mariani, (Eds.), Proceedings of the Second European Thermal Sciences Conference, Edizioni ETS, Pisa, Italy, 1996, pp. 1207–1213.
[17] M. Andreani, F. Putz, T.V. Dury, C. Gjerloev, B.L. Smith, On the application of field codes to the analysis of gas mixing in large volumes: case studies using CFX and GOTHIC, Ann. Nucl. Energy 30 (6) (2003) 685–714.
[18] Y.S. Choi, U.J. Lee, J.J. Lee, G.C. Park, Improvement of HYCA3D code and experimental verification in rectangular geometry, Nucl. Eng. Design 226 (2003) 337–349.
[19] S.V. Patankar, Numerical Heat Transfer and Fluid Flow, First ed., Hemisphere, NewYork, 1980.
[20] Z. Stosic, V. Stevanovic, Advanced three-dimensional two-fluid porous media method for transient two-phase flow thermal–hydraulics in complex geometries, Numer. Heat Transfer, Pt. B: Fund. 41 (2002) 263–289.
[21] X. Ji, J. Yan, Saturated thermodynamic properties for the air-water system at elevated temperatures and pressures, Chem. Eng. Sci. 58 (2003) 5069–5077.
[22] R. Bird, W.E. Stewart, E.N. Lightfoot, Transport Phenomena, First ed., Wiley, NewYork, 1960, p. 40.
[23] A. Bejan, Heat Transfer, First ed., Wiley, New York, 1993, pp. 398-405.
[24] C. Boyadjiev, V. Beschkov, Mass Transfer in Liquid Film Flows, First ed., Mir Publisher, Moscow, 1988, pp. 17–19.
[25] M.M. Chen, An analytical study of laminar film condensation: part 1—flat plates, J. Heat Transfer 83 (1961) 48–54.
[26] V. Stevanovic, M. Studovic, A simple model for vertical annular and horizontal stratified two-phase flows with liquid entrainment and phase transitions: one-dimensional steady-state conditions, Nucl. Eng. Design 154 (1995) 357–379.
[27] V. Stevanovic, An analytical model of gas absorption in open channel flow, Int. Commun. Heat Mass Transfer 24 (1997) 1187–1194.
[28] V.P. Isachenko, V.A. Osipova, A.S. Sukomel, Heat Transfer, Third ed., Mir Publishers, Moscow, 1980, pp. 278.
[29] E. Schmidt, Properties of water and steam in SI-units, First ed., Springer-Verlag, Berlin, 1969.
[30] J.P. Holman, Heat Transfer, Ninth ed., McGraw-Hill, New York, 1990, pp. 601-602.
[31] R.S. Reid, T.K. Sherwood, The Properties of Gases and Liquids, First ed., McGraw-Hill, New York, 1958.